ADVANCED OPTICAL MATERIALS
www.advopticalmat.de



# Unprecedented Thermo-Enhanced Retainable Circularly Polarized Luminescence

*Weilin Qi, Cheng Ma, Peilong Liao, Hongpeng Li, Ting Gu, Tongyue Wu, Jianbin Huang, and Yun Yan**

**Circularly polarized luminescence (CPL) enabled by chiral self-assembly is very promising in diversified applications. However, temperature-triggered disassembly or self-assembly transition often results in reduction or even silence of CPL. Here, a strategy of coordinating self-assembly is reported that offers temperature enhanced and retainable CPL that is resistant to further temperature variation. Upon co-assembling commercial dyes with the coordinating hydrogel of cholate-calcium, the chirality transfer from cholate to the dyes allows generation of CPL. With increasing temperature, the CPL intensity can be enhanced 4 times and the emission dissymmetry factor $g_{em}$ can be promoted from 0.04 to 0.1, then they remain stable either upon further elevating or lowering temperature. Mechanism study reveals that increasing temperature has triggered the coordination transition between the carbonate groups and $Ca^{2+}$ from the metastable bidentate chelating to the thermal stable bridging mode, which drives the transition from flexible nanohelices to stiff helical bunches. This promotes the alignment of the dyes and in the meantime decreases its mobility, thus leads to increased CPL intensity and $g_{em}$. It is envisioned that the strategy of coordinating self-assembly would be very promising in creating thermally stable CPL for diversified applications.**

## 1. Introduction

Circularly polarized luminescence (CPL) is very promising owing to their appealing applications in photoelectric devices,[1] chiroptical materials,[2] 3D displays,[3] and information storage.[4] Since CPL reflects the excited state properties of orderly arranged fluorescent molecules with specific chirality,[5] various chiral fluorescent molecules capable of self-assembling were created.[6] However, this usually requires complicated synthetic chemistry,[7] which can be tedious and poor yield[2a,8] if variation of the CPL color is required.

Recent study shows that chirality transfer is an alternative approach in constructing CPL materials.[2b,h,9] Upon co-assembling achiral chromophores with chiral ones which are easy to obtain, CPL can be facilely generated with diversified colors.[9b,10] Since there are judicious choice of achiral fluorescent molecules and diversified approaches leading to chiral supramolecular self-assemblies,[11] many extraordinary work manifesting amazing CPL have been created.[9b,10a,b,11c,12] In particular, chiral supramolecular assembly is able to amplify the chiroptical signal,[2e,9a,13] which is of critical importance in enhancing the efficiency of CPL for practical applications.

However, temperature-caused disassembly or self-assembly transition from large to small ones[4a,14] has protruded an insurmountable obstacle in the development of supramolecular CPL materials.[13a,15] CPL devices would inevitably generate heat or encounter high temperature environment in the course of service. In most cases, the molecular self-assembly becomes unstable with elevating temperature[14a,15c,16] due to the drastically enhanced solubility of the self-assembling molecules. For instance, upon increasing temperature, the wormlike micelles may transform into spherical ones,[17] and the crystalline self-assembly of microtubes would turn into spherical vesicles.[16a,18] Because the generation of CPL requires the fluorescent chromophores to orient toward a specific direction, disassembly or self-assembly transition from one-dimensional large structures to much smaller spherical ones usually causes CPL vanishing due to lose the ability to align fluorophores.[19] Up to date, it still remains challenging to endow supramolecular CPL materials with robust stability against variation of temperature.

In contrast to the temperature triggered disassembly, some coordinating hydrogels exhibit abnormal enhanced mechanical strength at elevated temperature.[20] Elegant examples can be found in the hydrogels formed with sodium cholate or folic acid and metal ions.[21] Specially, the sodium cholate (SC) is a naturally abundant chiral molecule which has no absorption in the UV–vis region. We therefore expect that the coordinating hydrogels formed with SC is an ideal chiral system to generate CPL with desired thermal-enhanced performance. Herein we report that this scenario indeed comes true upon co-assembling achiral fluorophores with the coordinating hydrogel formed with SC and $Ca^{2+}$. Different from most self-assembled noncovalent interactions that would be weakened by elevating

W. Qi, C. Ma, P. Liao, H. Li, T. Gu, T. Wu, J. Huang, Y. Yan
Beijing National Laboratory for Molecular Sciences (BNLMS)
State Key Laboratory for Structural Chemistry of Unstable and Stable Species
College of Chemistry and Molecular Engineering
Peking University
Beijing 100871, P. R. China
E-mail: yunyan@pku.edu.cn

The ORCID identification number(s) for the author(s) of this article can be found under https://doi.org/10.1002/adom.202201229.

**DOI: 10.1002/adom.202201229**

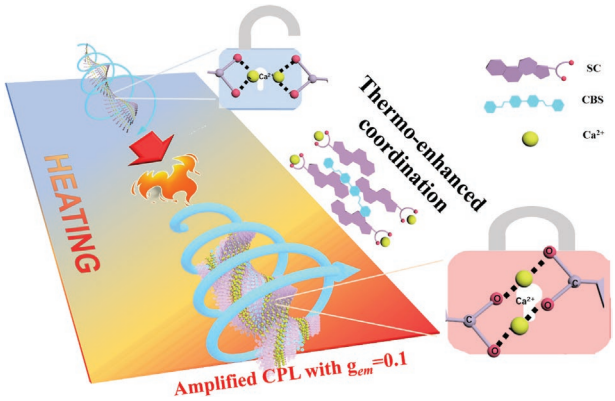


**Scheme 1.** Illustration of the thermo-enhanced CPL in SC-Ca-CBS hydrogel system.

temperature, the coordination between the carbonate groups and $Ca^{2+}$ changes from the metastable bidentate chelating to the thermal stable bridging mode upon increasing temperature (**Scheme 1**). As a consequence, the original individual SC-Ca nanohelices bunch together to form large-scale helical bundles. This not only decreases the mobility of the co-assembled fluorescent dyes, but also promotes their alignment. As a result, the CPL intensity is enhanced by about 4 times and the emission dissymmetry factor $g_{em}$ is enhanced from 0.04 to 0.1 as the temperature increases from 25 to 50 °C. Since the bridging coordination is thermal stable, further variation of temperature, no matter increasing or lowering it, would not change the high $g_{em}$ and CPL intensity any more. With this work, we demonstrate that thermal stable CPL can be obtained with the aid of coordinating self-assembly, which is very promising in the development of robust CPL materials.

## 2. Results and Discussion

The sodium cholate (SC)-calcium ($Ca^{2+}$) hydrogel established in literature[21a] was employed to co-assemble with the achiral fluorescent dye disodium 4,4′-bis(2-sulfostyryl) biphenyl (CBS)[1a,22] to generate CPL in this study. Stock solutions of 100 mM SC, 100 mM $Ca^{2+}$, and 20 mM CBS were mixed at the volume of 0.4, 0.4, and 0.01 mL, followed by addition of 1.19 mL distilled water. The resultant 2 mL transparent self-supporting SC-Ca-CBS (20-20-0.1 mM) hydrogel displayed bright blue fluorescence (**Figure 1**a). Microstructure study with AFM, TEM, and SEM revealed the formation of predominant flexible right-handed helices (Figure 1b,c and Figure S1, Supporting Information). The diameter for a single helix is about 10–40 nm with the pitches being about 70 nm (Figure 1c). Compared to the TEM image, the nano-helix under AFM has a relatively wider diameter. This originates from AFM tip broadening effect, which arises when the radius of curvature of the tip is comparable with, or greater than, the size of the object to be imaged.[23]

The size and morphology feature of the SC-Ca-CBS nanohelices is exactly the same with that of SC-Ca,[21a] indicating the addition of 0.1 mM CBS does not affect the gelation behavior. Indeed, rheology and XRD measurements confirm that both the mechanical strength and molecular packing mode are exactly the same in the SC-Ca-CBS and SC-Ca system (Figures S2 and S3, Supporting Information). However, CLSM image clearly shows the presence of luminescent fibers (Figure S4, Supporting Information), indicating CBS has been successfully incorporated into the SC-Ca helices. This is further evidenced by UV–vis measurements, which reveal that the absorption of CBS has red-shifted by about 3 nm (Figure 1d). 2D NMR NOESY (Nuclear Translimit Effect Spectroscopy) measurements are utilized to probe the interaction between molecules with small molecular weights. In line with UV–vis spectra, strong correlation was observed between the protons on CBS and the SC skeleton in 2D HNMR (NOESY) (Figure 1e). These results suggest that CBS molecules have inserted into the hydrophobic pocket formed by the face-to-face stacked SC molecules (Figure 1e).[24] Owing to the separation and confinement of the hydrophobic pocket, the absolute quantum yield (QY) of CBS was significantly enhanced from 62% in the 0.1 mM solution to 91% in the SC-Ca-CBS hydrogels. The confinement effect of a high rotational resistive microenvironment formed by SC-Ca gel effectively inhibited nonradiative decay, resulting in a remarkable increase in the QY.

The incorporation of CBS into the SC-Ca gels has triggered successful chirality transfer, namely, the chirality of the SC molecules transfers to the CBS dye through supramolecular interactions. As mentioned in the previous text, SC has no absorption in the entire UV–vis region measured, so that the CD signal is silent for the SC-Ca hydrogel. However, in the presence of achiral dye CBS, a distinct positive CD signal is observed at 370 nm (**Figure 2**a, blue line), corresponding to the absorption of CBS. The intensity of linear dichroism (LD) is nearly zero (Figure 2a, black line), thus the contribution of possible LD spectra on the CD signals can be excluded. Accordingly, a positive CPL of CBS peaked at 430 nm is observed (Figure 2b). The emission dissymmetry factor $g_{em}$, defined as $2(I_L - I_R)/(I_L + I_R)$, with $I_L$ and $I_R$ denoting the emission intensities of left-handed CPL (*l*-CPL) and right-handed CPL (*r*-CPL) component, respectively, is 0.04, indicating the generation of *l*-CPL. Since the $g_{em}$ of most organic fluorophores is in the order of $10^{-5}$–$10^{-3}$,[4b,25] while the alignment of them would significantly promote $g_{em}$ owing to the positive addition of the handedness,[6a,26] this fairly large $g_{em}$ value of 0.04 indicates that the CBS molecules have been orderly aligned in the nanohelices. During our CPL measurement, invariance of CPL amplitudes upon sample rotation (through successive 45° increments around the optical axis) and sample flipping (i.e., by turning it of 180° with respect to the vertical axis) was testified: in no cases we could observe significant variations.[27]

It is striking that the CPL displays temperature enhanced intensity and $g_{em}$. Figure 2b (upper panel) shows that with increasing temperature from 293 to 323 K, the CPL intensity has increased by nearly 4 times, whereas the fluorescence remains nearly unchanged (Figure 2b, lower panel). On the meanwhile, the maximum $g_{em}$ has been promoted by about 2.5 times, with the value increases from 0.04 to 0.1 (Figure 2c). This is in drastic contrast to the CPL reduction or silence triggered by increasing temperature in many other CPL systems.[15c,16a,b] In line with the temperature promoted CPL performance, the CD signal has been increased by the same amplitude (Figure 2a, upper panel), whereas the UV–vis absorbance (Figure 2a, lower panel)

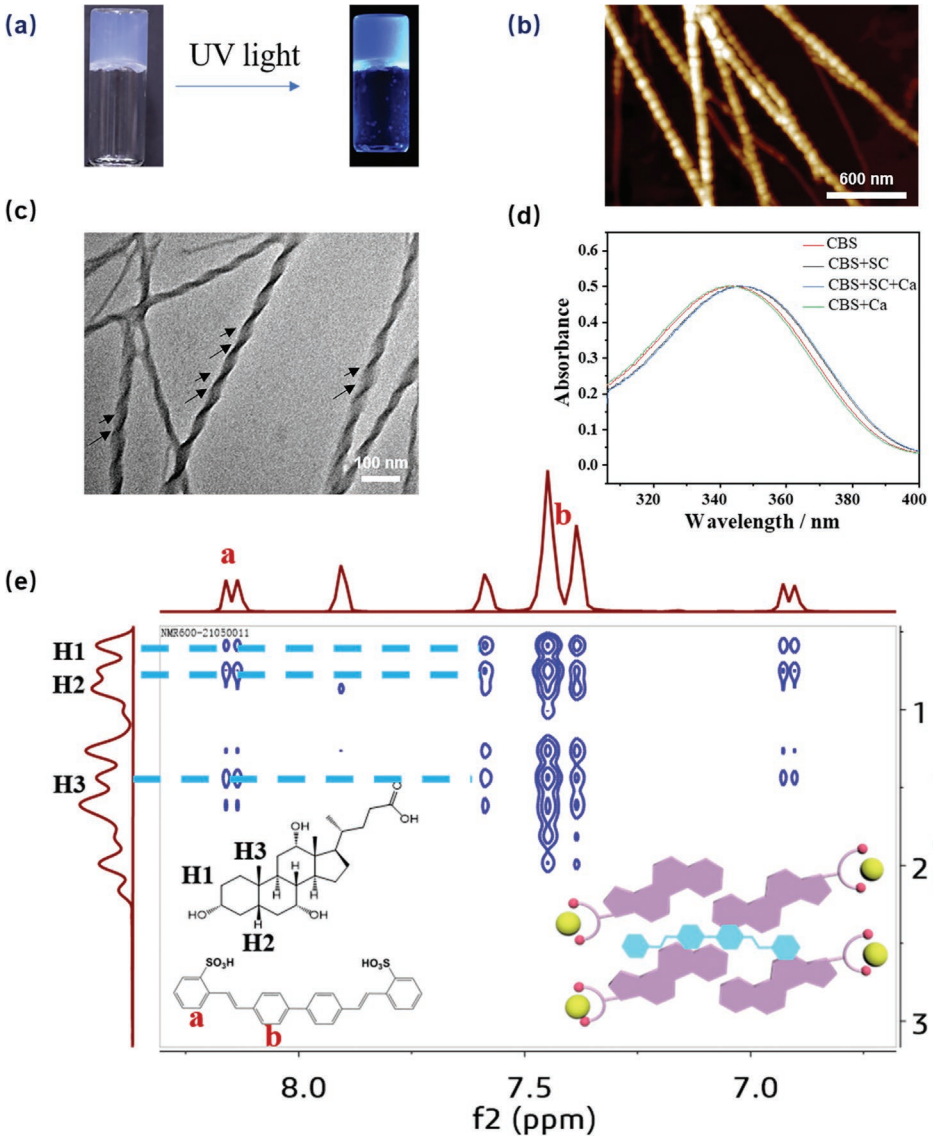


**Figure 1.** a) Photographs, b) AFM, c) TEM images, d) UV spectrum, e) 2D NMR (NOESY) of SC-Ca-CBS hydrogel systems employed in this study.

is not changed noticeably. This indicates that the enhanced CPL is originated from the better dipole–dipole coupling between CBS and SC. Meanwhile, Figure 2d shows that the storage modulus of the hydrogel has been enhanced 16 times, namely, increased from the original 6000 Pa at 293 K to 100 000 Pa at 323 K. This means that increasing temperature has triggered much stronger networks. It is noteworthy that the temperature-enhanced CPL and mechanical strength can be remembered by the system and remains stable in the broad temperature range of 293–343 K (Figures S5 and S6, Supporting Information). Figure 2c shows that the CPL intensity and the $g_{em}$ remains constant both in the process of further increasing temperature from 323 to 343 K (Figure 2c, red arrow) and decreasing temperature from 343 to 293 K (Figure 2c, green arrow).

Microstructure study with AFM and TEM reveals that the average diameter of the nanohelices increases from about 40 nm at 293 K to over 200 nm at 323 K (**Figure 3** and Figure S7, Supporting Information). The AFM image in Figure 3a shows that in many places, the widths of the helical bundles are over 600 nm at 323 K. These much larger helical bunches generate stronger scattering effect so that the turbidity of the hydrogel increased slightly (Figure S8, Supporting Information). Upon decreasing temperature, the turbidity would not recover, and microstructure study indicates that the helical bundles have been retained (Figure S9, Supporting Information). Furthermore, $^1$H NMR measurements (Figure S10, Supporting Information) manifest that the structure of the fluorophores remains unchanged in the hydrogel after heating to 323 K. Clearly, increasing temperature has significantly promoted the hierarchical self-assembly of the nanohelices, which not only leads to significantly enhanced mechanical strength of the resulting hydrogels, but also significantly rigidified the environment where the CBS has located, which accounts for the drastically enhanced CPL.

To unravel what have occurred at molecular level upon increasing temperature, FT-IR (Fourier transform infrared)

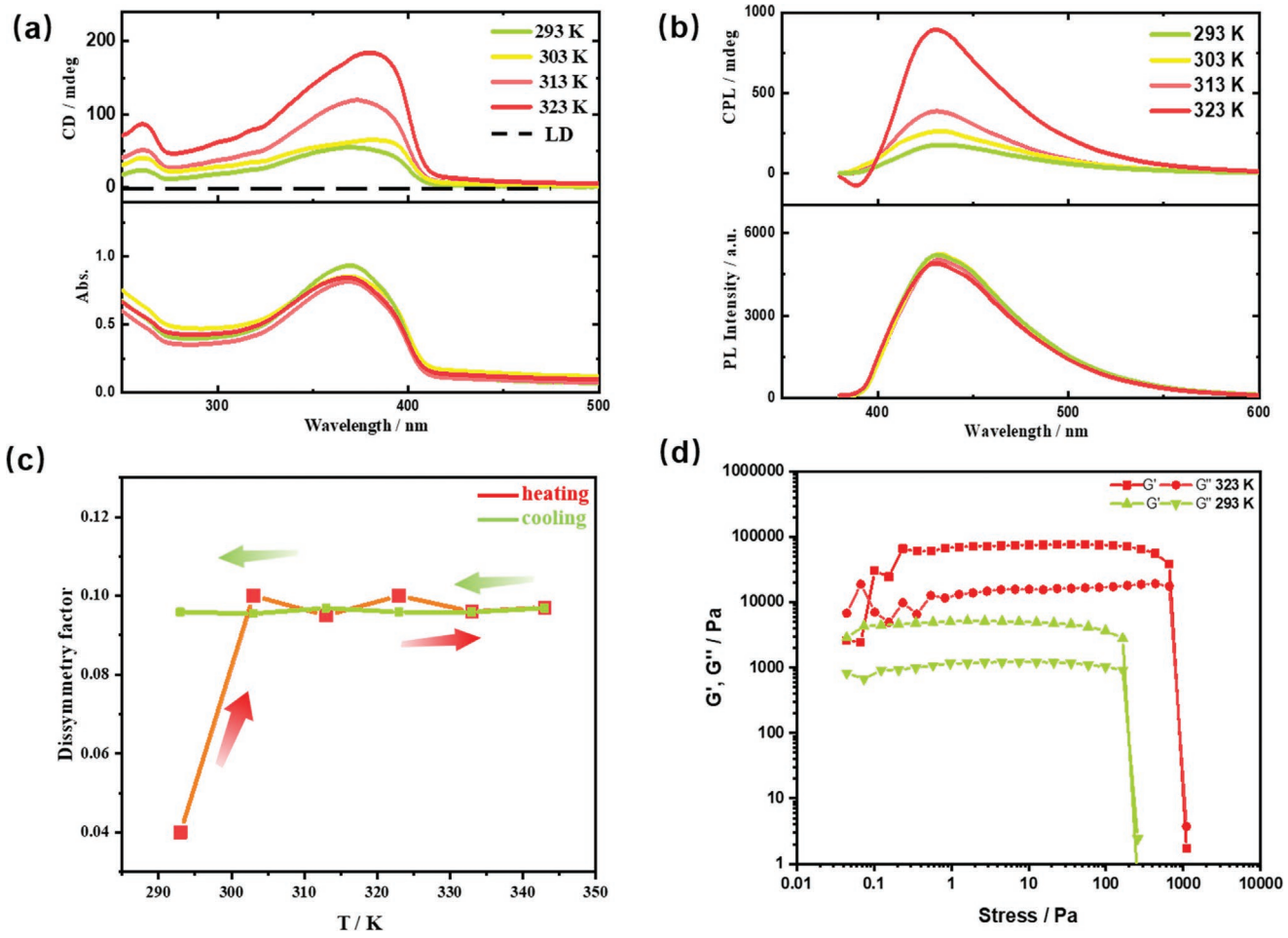


**Figure 2.** a) CD (upper) and UV–vis spectra (lower). LD is the linear dichroism signal. b) CPL (upper) and fluorescence spectra (lower), of the SC-Ca-CBS (20-20-0.1 mM) hydrogel at different temperatures. c) Variation of the dissymmetry factor ($g_{em}$) upon increasing temperature from 293 to 343 K and then decreasing from 343 to 293 K. d) Dynamic rheology profiles of the SC-Ca-CBS (20-20-0.1 mM) hydrogel at different temperatures.

measurements were conducted because it is able to distinct the coordination status between $Ca^{2+}$ and $–COO^-$ group.[21a] Elemental analysis, mass spectra and energy-dispersive spectroscopy (EDS) measurements have proved the molar ratio of SC:Ca is 1:1 in the hydrogel (Figures S11, S12 and Table S1, Supporting Information). **Figure 4**a shows that before heating, the symmetric and asymmetric vibration of the $–COO^-$ group in the SC-Ca system occur at 1424 and 1540 $cm^{-1}$ ($\Delta\nu$ = 116 $cm^{-1}$), respectively, whereas they shift to 1420 and 1555 $cm^{-1}$ ($\Delta\nu$ = 135 $cm^{-1}$) upon heating to 323 K. The $\Delta\nu$ value of 135 $cm^{-1}$ is close to that of SC single system ($\Delta\nu$ = 131 $cm^{-1}$, Figure S13, Supporting Information), whereas the $\Delta\nu$ of 116 $cm^{-1}$ is obviously smaller than SC. This means that at 293 K, $Ca^{2+}$ coordinate with the $–COO^-$ group of SC with a bidentate

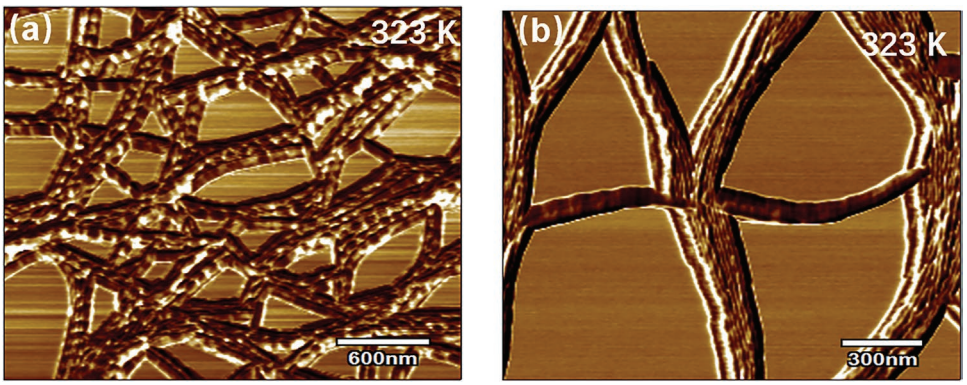


**Figure 3.** a,b) AFM images of the SC-Ca-CBS hydrogel system at 323 K.

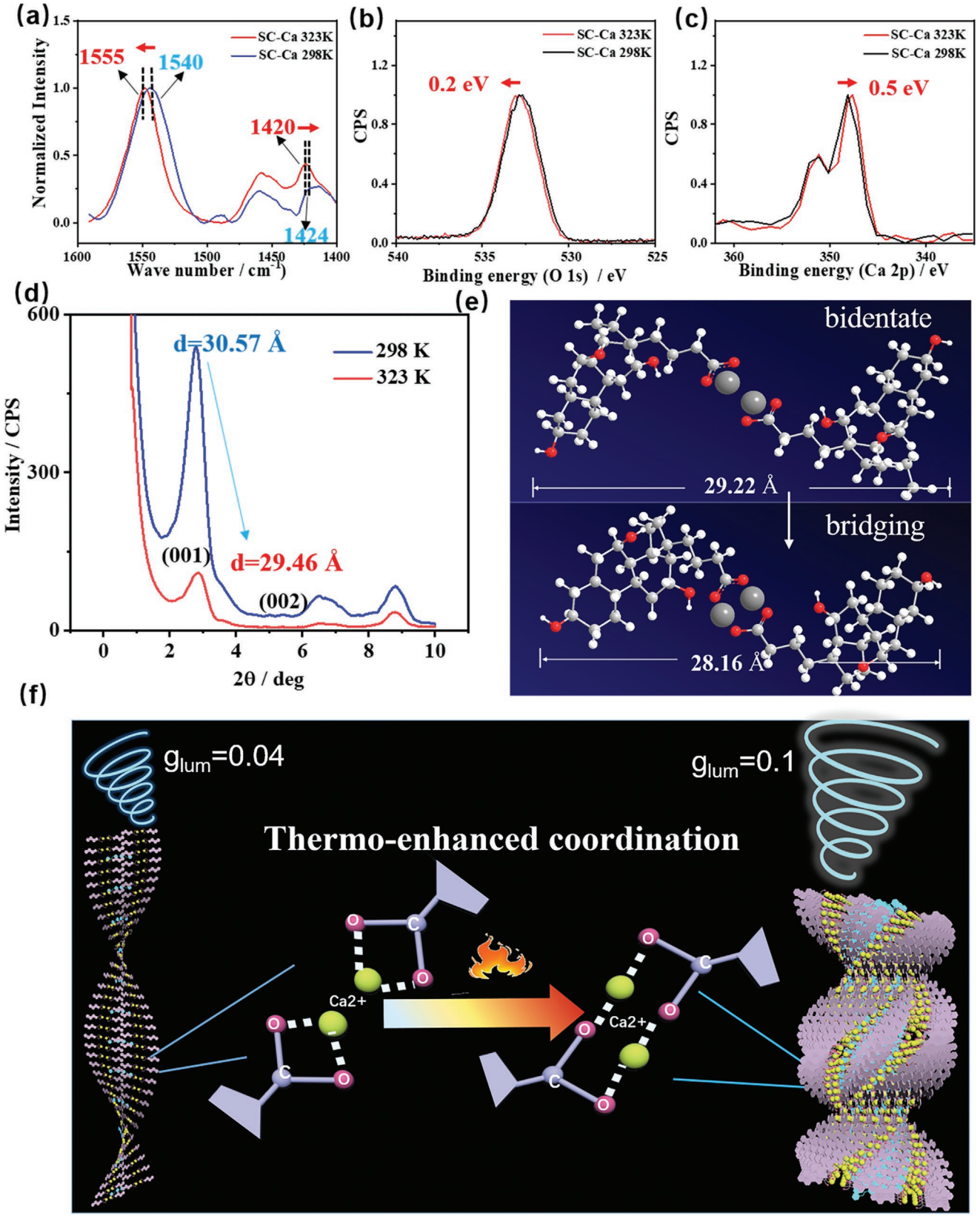


**Figure 4.** a) IR spectrum of SC-Ca gel before and after heating. XPS measurement of the binding energy of electrons for b) O 1s and c) Ca 2p of the SC-Ca hydrogel. d) XRD spectrum of SC-Ca-CBS hydrogel systems at 298 and 323 K, e) The bilayer thickness of the bidentate coordination and bridging coordination from Chem 3D. f) Schematic diagram of thermo-enhanced coordination and correlating morphological transformation from helix to helical bunches.

chelating mode, whereas increasing temperature has triggered the coordination between $-COO^-$ and $Ca^{2+}$ to change into bridging mode.[28] This can be further verified by the binding energy measurements of XPS (X-ray photoelectron spectroscopy). It reveals that upon increasing temperature the binding energy of O 1s has increased by 0.2 eV (Figure 4b), while that for $Ca^{2+}$ 2p electrons has decreased by 0.5 eV (Figure 4c). The variation of coordination mode from bidentate to bridging mode between SC and $Ca^{2+}$ has also changed the interlayer distances. As revealed by XRD measurements in Figure 4d, the interlayer distances, which is determined with the Bragg equation from the 001 diffraction, has been shortened from 30.57 Å at 293 K to 29.46 Å at 323 K. Since the interlayer distances is close to twice of the extending length of the SC molecules, this result manifests that the bridging coordination has effectively linked two SC skeleton via the coordination bond. Compared with the bilayers composed of two separated SC skeleton in the bidentate chelating mode, the bridging coordination have sewed the two SC skeleton together, which therefore has a shorter length, as revealed by the molecular modeling of Chem 3D (Figure 4e). The mechanism of the thermal enhanced and retainable CPL is illustrated in Figure 4f.

The current strategy of thermal triggered CPL enhancement can be extended to many other dyes. For example, as CBS was replaced by AC (Acridine yellow) or ThT (thioflavin T), thermal enhanced yellow (578 nm) and green (540 nm) CPL was observed, respectively (Figures S14 and S15, Supporting Information). However, dyes that has weak hydrophobic interactions with the SC-Ca hydrogels failed to display this temperature enhanced and remembered CPL (Figure S16, Supporting Information), indicating the hydrophobic interaction between dyes and the SC skeleton is very crucial to build this thermal enhanced CPL material.

## 3. Conclusions

Thermo-enhanced and retainable CPL with the high $g_{em}$ of 0.1 can be obtained by co-assembling commercial dyes with cholate-calcium hydrogels. The molecular reason lies in the thermo-promoted transition of the coordinating mode between $COO^-$ and $Ca^{2+}$ from bidentate chelating to bridging mode, which triggers the self-assembly transition from the separated nanohelix to the helical bundles. The dyes were further immobilized in the bundles which leads to better orientation and thermo-resistant fluorescence intensity. As a result, both the CPL intensity and $g_{em}$ are significantly enhanced. Since the bridging mode coordination is thermal stable, the thermal enhanced CPL is retainable, which stays constant with further variation of temperature. We envision that the coordinating self-assembly provides a facile route to construct thermal stable CPL materials with high $g_{em}$, which would pave the way for the practical application of CPL devices.

## 4. Experimental Section

*Materials*: Sodium cholate (SC, 99%), calcium nitrate tetrahydrate ($Ca(NO_3)_2{\cdot}4H_2O$, AR), disodium 4,4′-bis(2-sulfostyryl) biphenyl (CBS, AR) were purchased from Aladdin. Distilled water was purified through Milli-Q Advantage A10 Ultrapure Water System. $D_2O$ (99.9%) was purchased from Aldrich.

*Sample Preparation*: Hydrogel was conveniently obtained by mixing stock solutions of sodium cholate, calcium nitrate, and CBS and then equilibrated at 25 °C for one day before further analyses. During this period, a self-supporting hydrogel can form.

*Characterizations*: TEM images were captured with a JEM-100CX electron microscope. A drop of sample (about 30 µL) was loaded on a copper grid. SEM measurements were performed using a Hitachi S4800 microscope at an acceleration voltage of 1 kV. Energy-dispersive spectroscopy (EDS) measurement was conducted using the same instrument at an acceleration voltage of 7 kV. AFM measurements were performed on OXFORD INSTRUMENTS (Cypher S) in tapping mode. A drop (about 30 µL) of the sample was sealed between two slides, ready for CLSM observation. A TCS-sp inverted confocal laser scanning microscope (Leica, Germany) was used to conduct experiments in florescence and differential interference contrast (DIC) modes. Powder X-ray Diffraction (XRD) measurements were performed using a Rigaku Dmax-2400 diffractometer with Cu K$\alpha$ radiation. The powder samples were placed on clean glass slides for tests. The lamellar period $d$ in each sample was calculated using Bragg's Law, where $d = \lambda/2\sin\theta$. 1H-NMR and NOESY spectra experiments were performed on a Bruker ARX 500 MHz spectrometer at room temperature (25 ± 2°C), using 5 mm standard NMR tubes. Deuteroxide (99.9%) was used to dissolve the precipitates for 1 H-NMR spectra, all proton signals were calibrated with $D_2O$ signal at 4.800 ppm.; $D_2O$ (99.9%) was used to solve it for 2D-NOESY. Circular dichroism (CD) spectra were obtained on a JASCO J-810 spectrometer and used to investigate the ICD of the sample suspension. The light path length of the quartz cell used was 0.5 mm. Scanning speed was set at 100 nm $min^{-1}$. Data were collected at a response of 2 s and accumulated twice. CPL spectra were obtained with a JASCO CPL-200 spectrometer. The light path of the quartz cell was 0.5 mm. The excitation wavelength for ThT and RhB systems were both 400 nm. Fluorescence spectra were recorded by a FLS 920 spectrometer (Edinburgh Instruments Ltd., UK). The UV–vis absorption spectra were recorded on a Shimadzu UV-1800 spectrophotometer. The absolute fluorescent quantum yield (FQY) of the SC-Ca-CBS hydrogels were conducted using Edinburgh instruments, FLS980 with R928PMT as the detector, a 450 W xenon lamp as the light source, and an integrating sphere accessory. The excitation wavelength was 340 nm. FT-IR spectra were carried out on Nicolet iN10 MX microscopic infrared spectrometer (ThermoS-7 Scientific Co., USA) in the range of 4000 to 600 $cm^{-1}$ under ambient condition. The spectrometer was equipped with an attenuated total reflection (ATR) accessory with a Smart iTR (diamond). Electrospray ionization mass spectrometry (ESI-MS) was carried out on an APEX IV FT-MS (Bruker, USA). The operating conditions of the ESI source: positive ion mode; spray voltage 3300 V; capillary voltage 3800 V, capillary temperature 30 °C; skimmer1 33.0 V, skimmer2 28.0 V; sheath gas nitrogen pressure 0.3 bar. An elemental analyzer (virioEL, Elementar Analysensysteme GmbH company) was used to measure the contents of C, H, and N elements. An Inductively Coupled Plasma-Atomic Emission Spectrometer (Prodigy 7, Leeman, USA) was used to measure the contents of Ca element. When lowering the concentration of solutions of sodium cholate and calcium nitrate to 10 mM, precipitation not gel could be obtained. TEM revealed that the precipitates are composed of right-handed helices the same as those in gel. Therefore, the precipitates were collected by removal of the supernatants and lyophilized for further constitutional analysis in assemblies.

*Molecular Modeling*: The molecular model proposed in Figure 4e was designed and built according to the XRD, XPS, and IR results and utilized to visualize the change of coordinating mode. The geometry optimization was performed under MM2 force field by Chem3D 19.1 minimize energy calculation with minimum RMS gradient of 0.0100. ESI-MS spectra in Figure S11 (Supporting Information) had showed the presence of $[SC\text{-}Ca\text{-}HNO_3]^+$ and $[SC\text{-}Ca\text{-}H_2O]^+$, which proved there are $NO_3^-$ and $H_2O$ coordinating groups surrounding $Ca^{2+}$, which could

neutralize and separate $Ca^{2+}$, thus electrostatic repulsion was negligible in the neutral system.

The coordination between $Ca^{2+}$ and CBS was ignored for carboxyl (SC) and had stronger coordinating ability than sulfonate (CBS) with $Ca^{2+}$. Meanwhile, the ratio of CBS to SC was 1:200. Therefore, it was thought that the coordination between CBS and $Ca^{2+}$ was negligible.

## Supporting Information

Supporting Information is available from the Wiley Online Library or from the author.

## Acknowledgements

The authors are grateful to National Natural Science Foundation of China (Grant Nos. 22172004, 21972003) and the Beijing National Laboratory for Molecular Sciences (BNLMS) for financial support.

## Conflict of Interest

The authors declare no conflict of interest.

## Author Contributions

W.Q. carried out most of the experiments and drafted this paper. C.M. composed the cartoons of the assemblies. P.L., H.L., T.G., and T.W. helped with the methodology of the experiments. J.H. helped to discuss and analyze the results. Y.Y. designed the work and wrote up the paper. All authors have given approval to the final version of the manuscript.

## Data Availability Statement

The data that support the findings of this study are available from the corresponding author upon reasonable request.

## Keywords

chirality transfer, circularly polarized luminescence, coordination interaction, heat-promoted hydrogel, supramolecular self-assembly

Received: May 28, 2022
Revised: September 29, 2022
Published online:

[1] a) C. Zhang, Z. P. Yan, X. Y. Dong, Z. Han, S. Li, T. Fu, Y. Y. Zhu, Y. X. Zheng, Y. Y. Niu, S. Q. Zang, *Adv. Mater.* **2020**, *32*, 2002914; b) Y. H. Kim, Y. Zhai, E. A. Gaulding, S. N. Habisreutinger, T. Moot, B. A. Rosales, H. Lu, A. Hazarika, R. Brunecky, L. M. Wheeler, J. J. Berry, M. C. Beard, J. M. Luther, *ACS Nano* **2020**, *14*, 8816; c) R. Carr, N. H. Evans, D. Parker, *Chem. Soc. Rev.* **2012**, *41*, 7673; d) W. Zhao, Y. Wang, S. Wan, H. Lu, M. Li, C. Chen, *CCS Chem.* **2022**, https://doi.org/10.31635/ccschem.021.202101509.

[2] a) Y. Ru, L. Sui, H. Song, X. Liu, Z. Tang, S. Q. Zang, B. Yang, S. Lu, *Angew. Chem.* **2021**, *133*, 14210; *Angew. Chem., Int. Ed. Engl.* **2021**, *60*, 14091; b) S. Ma, J. Jiang, Z. Liu, Y. Jiang, Z. Wu, M. Liu, *Nanoscale* **2020**, *12*, 7895; c) B. Zhao, X. Gao, K. Pan, J. Deng, *ACS Nano* **2021**, *15*, 7463; d) Q. Xia, L. Meng, T. He, G. Huang, B. S. Li, B. Z. Tang, *ACS Nano* **2021**, *15*, 4956; e) E. M. Sanchez Carnerero, A. R. Agarrabeitia, F. Moreno, B. L. Maroto, G. Muller, M. J. Ortiz, S. de la Moya, *Chem. - Eur. J.* **2015**, *21*, 13488; f) A. M. K. Velmurugan, A. Saeed, J. Li, K. Wang, M. Zuo, Q. Liu, X. Hu, *CCS Chem.* **2022**, *4*, 3426; g) F. Wang, F. Gan, G. Zhang, H. Qiu, *CCS Chem.* **2022**, https://doi.org/10.31635/ccschem.022.202202024; h) C. Lin, K. L. Y. Duan, H. Duan, Y. Li, M. Gao, L. Cao, *CCS Chem.* **2020**, *2*, 2749.

[3] a) O. Oki, C. Kulkarni, H. Yamagishi, S. C. J. Meskers, Z. H. Lin, J. S. Huang, E. W. Meijer, Y. Yamamoto, *J. Am. Chem. Soc.* **2021**, *143*, 8772; b) M. Khorloo, X. Yu, Y. Cheng, H. Zhang, S. Yu, J. W. Y. Lam, M. Zhu, B. Z. Tang, *ACS Nano* **2021**, *15*, 1397.

[4] a) H. Jiang, Y. Jiang, J. Han, L. Zhang, M. Liu, *Angew. Chem.* **2019**, *131*, 795; *Angew. Chem., Int. Ed. Engl.* **2019**, *58*, 785; b) L. Zhang, H. X. Wang, S. Li, M. H. Liu, *Chem. Soc. Rev.* **2020**, *49*, 9095; c) Q. Xia, W. Xie, T. He, H. Zhang, Z. Zhao, G. Huang, B. Li, B. Tang, *CCS Chem.* **2022**, https://doi.org/10.31635/ccschem.022.202202173.

[5] J. P. Riehl, F. S. Richardson, *Chem. Rev.* **1986**, *86*, 1.

[6] a) F. Wang, H. Qiu, C. Feng, *Adv. Funct. Mater.* **2020**, *30*, 2002936; b) F. Wang, W. Ji, P. Yang, C. L. Feng, *ACS Nano* **2019**, *13*, 7281; c) P. Liao, S. Zang, T. Wu, H. Jin, W. Wang, J. Huang, B. Z. Tang, Y. Yan, *Nat. Commun.* **2021**, *12*, 5496; d) Y. He, S. Zhang, H. K. Bisoyi, J. Qiao, H. Chen, J. Gao, J. Guo, Q. Li, *Angew. Chem.* **2021**, *133*, 27364; *Angew. Chem., Int. Ed. Engl.* **2021**, *60*, 27158; e) Q. Ye, F. Zheng, E. Zhang, H. K. Bisoyi, S. Zheng, D. Zhu, Q. Lu, H. Zhang, Q. Li, *Chem. Sci.* **2020**, *11*, 9989.

[7] a) Y. Ru, L. Ai, T. Jia, X. Liu, S. Lu, Z. Tang, B. Yang, *Nano Today* **2020**, *34*, 100953; b) L. Dordevic, F. Arcudi, A. D'Urso, M. Cacioppo, N. Micali, T. Buergi, R. Purrello, M. Prato, *Nat. Commun.* **2018**, *9*, 3442; c) H. Wu, X. He, B. Yang, C. C. Li, L. Zhao, *Angew. Chem.* **2021**, *133*, 1559; *Angew. Chem., Int. Ed. Engl.* **2021**, *60*, 1535.

[8] Z. Q. Li, Z. L. Gong, J. Y. Shao, J. Yao, Y. W. Zhong, *Angew. Chem.* **2021**, *133*, 14716; *Angew. Chem., Int. Ed. Engl.* **2021**, *60*, 14595.

[9] a) T. Goto, Y. Okazaki, M. Ueki, Y. Kuwahara, M. Takafuji, R. Oda, H. Ihara, *Angew. Chem.* **2017**, *129*, 3035; *Angew. Chem., Int. Ed. Engl.* **2017**, *56*, 2989; b) W. Shang, X. Zhu, T. Liang, C. Du, L. Hu, T. Li, M. Liu, *Angew. Chem.* **2020**, *132*, 12911; *Angew. Chem., Int. Ed. Engl.* **2020**, *59*, 12811; c) C. Du, X. Zhu, C. Yang, M. Liu, *Angew. Chem.* **2022**, *134*, e202113979; *Angew. Chem., Int. Ed. Engl.* **2022**, *61*, 202113979.

[10] a) J. Kumar, T. Nakashima, T. Kawai, *J. Phys. Chem. Lett.* **2015**, *6*, 3445; b) J. F. Chen, X. Yin, B. Wang, K. Zhang, G. Meng, S. Zhang, Y. Shi, N. Wang, S. Wang, P. Chen, *Angew. Chem.* **2020**, *132*, 11363; *Angew. Chem., Int. Ed. Engl.* **2020**, *59*, 11267; c) L. Wang, A. M. Urbas, Q. Li, *Adv. Mater.* **2020**, *32*, 1801335.

[11] a) W. Miao, D. Yang, M. Liu, *Chem. - Eur. J.* **2015**, *21*, 7562; b) A. Sorrenti, R. R. Trujillo, D. B. Amabilino, J. Puigmarti Luis, *J. Am. Chem. Soc.* **2016**, *138*, 6920; c) H. Wang, H. K. Bisoyi, B. X. Li, M. E. McConney, T. J. Bunning, Q. Li, *Angew. Chem.* **2020**, *132*, 2706; *Angew. Chem., Int. Ed. Engl.* **2020**, *59*, 2684.

[12] J. Liang, P. Guo, X. Qin, X. Gao, K. Ma, X. Zhu, X. Jin, W. Xu, L. Jiang, P. Duan, *ACS Nano* **2020**, *14*, 3190.

[13] a) F. Wang, F. Gan, C. Shen, H. Qiu, *J. Am. Chem. Soc.* **2020**, *142*, 16167; b) L. Yang, J. Huang, M. Qin, X. Ma, X. Dou, C. Feng, *Nanoscale* **2020**, *12*, 6233.

[14] a) F. Wang, M. Qin, T. Peng, X. Tang, A. Y. Dang i, C. Feng, *Langmuir* **2018**, *34*, 7869; b) Q. Cheng, A. Hao, P. Xing, *Adv. Colloid Interface Sci.* **2020**, *286*, 102301; c) V. Krishnasamy, W. Qu, C. Chen, H. Huo, K. Ramanagul, V. Gothandapani, G. H. Mehl, Q. Zhang, F. Liu, *Macromolecules* **2020**, *53*, 4193; d) R. D. Mukhopadhyay, G. Das, A. Ajayaghosh, *Nat. Commun.* **2018**, *9*, 1987.

[15] a) P. Duan, Y. Li, L. Li, J. Deng, M. Liu, *J. Phys. Chem. B* **2011**, *115*, 3322; b) Y. Chen, P. Lu, Z. Li, Y. Yuan, Q. Ye, H. Zhang, *ACS Appl.*

*Mater. Interfaces* **2020**, *12*, 56604; c) P. Lu, Y. Chen, Z. Chen, Y. Yuan, H. Zhang, *J. Mater. Chem. C* **2021**, *9*, 6589.

[16] a) X. Wang, W. Zhi, C. Ma, Z. Zhu, W. Qi, J. Huang, Y. Yan, *JACS Au* **2021**, *1*, 156; b) Y. Zhao, X. Zhang, W. Li, A. Zhang, *Eur. Polym. J.* **2019**, *118*, 275; c) C. Kulkarni, P. A. Korevaar, K. K. Bejagam, A. R. A. Palmans, E. W. Meijer, S. J. George, *J. Am. Chem. Soc.* **2017**, *139*, 13867; d) Z. B. Sun, J. K. Liu, D. F. Yuan, Z. H. Zhao, X. Z. Zhu, D. H. Liu, Q. Peng, C. H. Zhao, *Angew. Chem.* **2019**, *131*, 4894; *Angew. Chem., Int. Ed. Engl.* **2019**, *58*, 4840; e) K. Akagi, T. Yamashita, K. Horie, M. Goh, M. Yamamoto, *Adv. Mater.* **2020**, *32*, 1906665.

[17] a) Z. Li, W. Kang, Y. Zhao, H. Yang, M. Li, X. Kang, T. Zhu, B. Zhou, B. Sarsenbekuly, S. Aidarova, *J. Colloid Interface Sci.* **2022**, *608*, 893; b) Y. Lin, Y. Qiao, Y. Yan, J. Huang, *Soft Matter* **2009**, *5*, 3047.

[18] a) C. Zhou, X. Cheng, Y. Yan, J. Wang, J. Huang, *Langmuir* **2014**, *30*, 3381; b) Y. Zhou, S. Wang, M. Lv, B. Xu, F. Han, L. Zhao, *J. Dispersion Sci. Technol.* **2018**, *39*, 1056.

[19] a) Y. Deng, M. Wang, Y. Zhuang, S. Liu, W. Huang, Q. Zhao, *Light: Sci. Appl.* **2021**, *10*, 76; b) K. Ma, W. Chen, T. Jiao, X. Jin, Y. Sang, D. Yang, J. Zhou, M. Liu, P. Duan, *Chem. Sci.* **2019**, *10*, 6821.

[20] a) V. Tournier, C. M. Topham, A. Gilles, B. David, C. Folgoas, E. M. Leclair, E. Kamionka, M. L. Desrousseaux, H. Texier, S. Gavalda, M. Cot, E. Guemard, M. Dalibey, J. Nomme, G. Cioci, S. Barbe, M. Chateau, I. Andre, S. Duquesne, A. Marty, *Nature* **2020**, *580*, 216; b) J. Brassinne, J. P. Bourgeois, C. A. Fustin, J. F. Gohy, *Soft Matter* **2014**, *10*, 3086.

[21] a) Y. Qiao, Y. Lin, Y. Wang, Z. Yang, J. Liu, J. Zhou, Y. Yan, J. Huang, *Nano Lett.* **2009**, *9*, 4500; b) K. Liu, C. Ma, W. Wang, S. Zang, Y. Cai, W. Chen, Z. Liu, J. Huang, Y. Yan, *Inorg. Chem. Front.* **2020**, *7*, 4086; c) S. Basak, I. Singh, A. Banerjee, H. B. Kraatz, *RSC Adv.* **2017**, *7*, 14461; d) H. Jin, Y. Cai, H. Li, P. Liao, T. Wu, C. Ma, Q. Chen, Q. Qian, J. Huang, Y. Yan, *Adv. Opt. Mater.* **2022**, *10*, 2200130.

[22] a) S. Canonica, J. B. Kramer, D. Reiss, H. Gygax, *Environ. Sci. Technol.* **1997**, *31*, 1754; b) J. M. Kesselman Truttmann, S. J. Hug, *Environ. Sci. Technol.* **1999**, *33*, 3171; c) A. Abbasi, M. Eslamian, D. Heyd, D. Rousseau, *Pharm. Dev. Technol.* **2008**, *13*, 549; d) J. M. Dyer, C. D. Cornellison, S. D. Bringans, G. Maurdev, K. R. Millington, *Photochem. Photobiol.* **2008**, *84*, 145; e) M. Takahashi, K. Kawamura, *Water, Air, Soil Pollut.* **2007**, *180*, 39.

[23] P. Samori, V. Francke, T. Mangel, K. Mullen, J. P. Rabe, *Opt. Mater.* **1998**, *9*, 390.

[24] M. Zhang, X. Yin, T. Tian, Y. Liang, W. Li, Y. Lan, J. Li, M. Zhou, Y. Ju, G. Li, *Chem. Commun.* **2015**, *51*, 10210.

[25] M. H. Liu, L. Zhang, T. Y. Wang, *Chem. Rev.* **2015**, *115*, 7304.

[26] a) B. Wu, H. Wu, Y. Zhou, D. Zheng, X. Jia, L. Fang, L. Zhu, *Angew. Chem.* **2021**, *133*, 3716; *Angew. Chem., Int. Ed. Engl.* **2021**, *60*, 3672; b) B. Li, Y. Li, M. H. Y. Chan, V. W. W. Yam, *J. Am. Chem. Soc.* **2021**, *143*, 21676; c) J. J. Wang, H. T. Zhou, J. N. Yang, L. Z. Feng, J. S. Yao, K. H. Song, M. M. Zhou, S. Jin, G. Zhang, H. B. Yao, *J. Am. Chem. Soc.* **2021**, *143*, 10860.

[27] a) G. Albano, L. A. Aronica, A. Minotto, F. Cacialli, L. Di Bari, *Chem. -Eur. J.* **2020**, *26*, 16622; b) T. Ikeda, T. Masuda, T. Hirao, J. Yuasa, H. Tsumatori, T. Kawai, T. Haino, *Chem. Commun.* **2012**, *48*, 6025; c) R. Kuroda, T. Harada, Y. Shindo, *Rev. Sci. Instrum.* **2001**, *72*, 3802.

[28] a) H. Xie, Z. Li, J. Gong, L. Hu, P. Alam, X. Ji, Y. Hu, J. H. C. Chau, J. W. Y. Lam, R. T. K. Kwok, B. Z. Tang, *Adv. Mater.* **2021**, *33*, 2105113; b) M. Nara, H. Torii, M. Tasumi, *J. Phys. Chem.* **1996**, *100*, 19812; c) S. Mizushima, I. Ichishima, I. Nakagawa, J. V. Quagliano, *J. Phys. Chem.* **1955**, *59*, 293; d) G. B. Deacon, R. J. Phillips, *Coord. Chem. Rev.* **1980**, *33*, 227; e) Y. Lan, L. Xu, Y. Yan, J. Huang, A. de Keizer, N. A. M. Besseling, M. A. C. Stuart, *Soft Matter* **2011**, *7*, 3565; f) H. L. Gao, B. Ding, L. Yi, P. Cheng, D. Z. Liao, S. P. Yan, Z. H. Jiang, *Inorg. Chem. Commun.* **2005**, *8*, 151.